
This is an electronic reprint of the original article.
This reprint may differ from the original in pagination and typographic detail.

Vaimann, Toomas; Sobra, Jan; Belahcen, Anouar; Rassõlkin, Anton; Rolak, Michal; Kallaste, Ants

Induction machine fault detection using smartphone recorded audible noise

Published in:
IET Science Measurement and Technology

DOI:
[10.1049/iet-smt.2017.0104](https://doi.org/10.1049/iet-smt.2017.0104)

Published: 01/07/2018

Document Version
Peer-reviewed accepted author manuscript, also known as Final accepted manuscript or Post-print

Please cite the original version:
Vaimann, T., Sobra, J., Belahcen, A., Rassõlkin, A., Rolak, M., & Kallaste, A. (2018). Induction machine fault detection using smartphone recorded audible noise. *IET Science Measurement and Technology*, 12(4), 554-560. <https://doi.org/10.1049/iet-smt.2017.0104>

This material is protected by copyright and other intellectual property rights, and duplication or sale of all or part of any of the repository collections is not permitted, except that material may be duplicated by you for your research use or educational purposes in electronic or print form. You must obtain permission for any other use. Electronic or print copies may not be offered, whether for sale or otherwise to anyone who is not an authorised user.

Induction Machine Fault Detection Using Smartphone Recorded Audible Noise

Toomas Vaimann^{1,*}, Jan Sobra², Anouar Belahcen^{1,3}, Anton Rassõlkin¹, Michal Rolak⁴, Ants Kallaste¹

¹ Department of Electric Power Engineering and Mechatronics, Tallinn University of Technology, Tallinn, Estonia

² Department of Electromechanics and Power Electronics, University of West Bohemia, Plzen, Czech Republic

³ Department of Electrical Engineering and Automation, Aalto University, Aalto, Finland

⁴ Institute of Control and Industrial Electronics, Warsaw University of Technology, Warsaw, Poland

*toomas.vaimann@tu.ee

Abstract: This paper presents induction machine fault detection possibilities using smartphone recorded audible noise. Different faults of the induction machine, such as various numbers of broken rotor bars and rotor eccentricities are inflicted to the machine. Analysis is performed on audible noise recorded by two different smartphones and compared with mechanical vibrations recorded by sensors. Neural network is composed and probabilities of fault detection using such diagnostic measures are presented. Necessity for further study is pointed out.

1. Introduction

Various methods of fault detection are used in electrical machine diagnostics today. The time-frequency signal processing based condition monitoring methods, such as the short-time Fourier transform [1], [2], the wavelet transform [3]-[7], the empirical mode decomposition [8]-[12], and the Hilbert-Huang transform [13]-[15], have been extensively used with current, vibration, and acoustic emission signals to detect the diverse symptoms of motor failures [16]. Such methods are often used for the diagnostic purposes of the electric machines, but they have often been criticized for being limited by their complexity, and their time consumption as well as the needed computing resource, to be used in real-time applications [17]-[19].

Another problem is the cost, complexity of use and limitation of condition monitoring tools and devices. Most industries, where electrical machines are performing high responsibility tasks, are in a need of condition monitoring and diagnostic approaches. In many cases however the cost of installing condition monitoring system, might be difficult to justify on noncritical machinery due to potentially long payback period on the investment [20].

A simple tool for performing, at least preliminary, condition monitoring and control for the electrical machines could be the smartphone, or practically any mobile device with the ability of recording sound. This is a promising direction in simplification and wider availability of diagnostic tools in the market. So far, not too many research papers have been dedicated to electrical machine diagnostics through the medium of mobile phones. One of the latest and experimentally verified papers is [20], where only the detection of bearing faults with the help of a mobile phone is investigated.

The given paper deals with experiments and computations to prove the usability of smartphones for simple condition monitoring procedures in case of various electrical machine faults. The aim of the paper is to show the applicability of mobile phones as devices for pre-determination of potentially faulty electrical machines.

2. Measurements and methods

Different faults were inflicted to the induction machine under investigation. The data of the investigated motor is presented in Table 1 and the schematic of the experimental setup is shown in Fig. 1.

The measured conditions of the machine are as follows:

1. One broken rotor bar;
2. Two consecutive broken rotor bars;
3. Two broken rotor bars with four healthy ones in between;
4. Three consecutive broken rotor bars;
5. Dynamic eccentricity with two non-consecutive broken rotor bars;
6. Dynamic eccentricity with two non-consecutive broken rotor bars and loose bearing;
7. Dynamic eccentricity;
8. Healthy machine.

Broken rotor bars were implemented by simply drilling a hole through respective number of rotor bars. For the dynamic eccentricity, the rotor was shifted 28% of the air-gap length using an additional ring between the shaft and the bearing. Loose bearing situation was achieved by using a slightly larger inner diameter bearing.

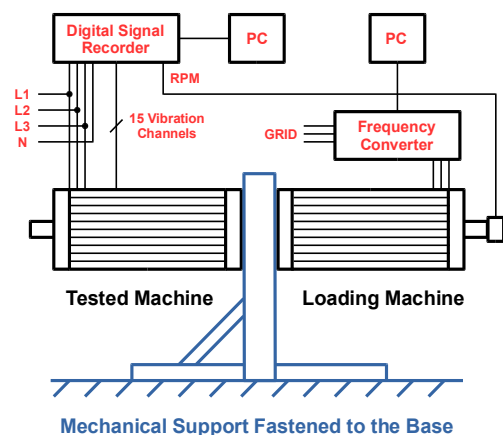


Fig. 1. Schematic of the experimental setup

Table 1 Data of the investigated induction machine

Parameter	Symbol	Value
Rated voltage	U_n	400V@60 Hz; 333V@50 Hz
Rated current	I_n	41 A
Rated speed	n_n	1680 rpm@60 Hz; 1400 rpm@50 Hz
Rated power	P_n	22 kW@60 Hz; 18 kW@50 Hz
Frequency	f	50-60 Hz
Power factor	$\cos\phi$	0.86
Number of poles	$2p$	4
Number of rotor bars	Q_r	40
Number of stator slots	Q_s	48

During the experiments, all electric data of the induction machine under investigation was measured as well as the mechanical vibrations were recorded using five three-axial vibration sensors mounted on the circumference of the machine. Audible noise of the machine was measured using two different smartphones from six different positions around the tested motor one meter away from the surface of the machine. The resulting sound files were analysed and audible noise vibrations were compared to mechanical vibration data. Positions for mechanic and audible noise vibration measurements are shown on Fig. 2.

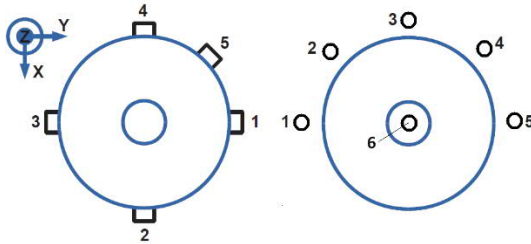


Fig. 2. Schematic of the front view of the tested machine. Left – vibration sensors' mounting positions on the surface of the machine; right – smartphone recording positions in the distance of 1 m from the surface of the machine

Smartphones, used for the experimental purposes, were selected to be not the newest models, but widely available, and of average price and quality range. The selected phone brands were Sony Xperia GO and Samsung Galaxy S4 mini. Built in recorder of the phones was used to record the sound of the operational induction machine. The sound files were not additionally filtered, however, it is difficult to say, to what extent the phones' built in filter is changing the recorded sound as such information is not publicly available from the manufacturers.

3. Characteristic fault related frequencies

3.1. Rotational speed frequency

Rise of vibrations at the rotational speed frequency and/or its harmonics is characteristic for different faults including dynamic eccentricity, broken rotor bars and loose bearing. Dynamic eccentricity leads to the non-uniform air-gap length around the stator circumference. That results in greater magnetic force acting in the direction of minimal air-gap, which can be referred to as the unbalanced magnetic pull. Since the position of the minimal air-gap is changing with revolving rotor, unbalanced magnetic pull excites the vibration at the rotor speed frequency (1) [21], [22].

$$f_{cx} = c \frac{RPM}{60} \quad c = 1, 2, 3, \dots \quad (1)$$

Current termination in broken rotor bar results in leakage flux extinction around that bar. Then, rotor tooth next to broken bar in direction of rotation is oversaturated and relatively large radial force originates in the area. This force rotates around the air-gap and creates unbalanced magnetic pull, similarly as dynamic eccentricity does. Moreover the current, originally flowing in the broken bar, splits amongst neighbouring bars, which leads to the temperature rise in these bars [23].

In case of rotor eccentricity and broken rotor bars, several sidebands shifted of pole passing frequency (2) multiples can occur around the particular rotational speed harmonics. The sidebands are the product of amplitude and frequency modulations [24].

$$f_p = 2pf_s, \quad (2)$$

In (2) p is the number of pole pairs and f_s is the slip frequency of the machine.

Both dynamic eccentricity and broken rotor bars are faults of electromagnetic origin and vibrations at rotational speed frequencies drop immediately after the power cut. In case of loose bearing, vibration at these frequencies disappears at lower speed. While dynamic eccentricity and broken rotor bars excite vibrations mainly at f_{1x} , for loose bearing more characteristic vibrations are at f_{2x} and f_{3x} .

3.2. Twice line frequency

Twice line frequency f_{2L} vibrations of the machine are caused by radial magnetic forces acting on the stator teeth and core as well as magnetostriction. Values of the radial forces are derived from the air-gap flux density distribution and they vary in space and time [22]:

$$p_m(\alpha, t) = \frac{B^2(\alpha, t)}{2\mu_0}, \quad (3)$$

where p_m is the surface magnetic force density in the particular time instant t and angular position around stator circumference α , B is the corresponding flux density and μ_0 is the permeability of free space.

Considering sinusoidal magnetizing current, the resulting force has two peak values in each current period – at the positive and the negative maximum value. This means, that vibrations caused by this force have frequency equal to twice the frequency of the supplying current. It is obvious that certain vibrations at twice line frequency are excited even in healthy machines. Vibrations at this frequency are typical for static eccentricity but sometimes can be excited by dynamic eccentricity as well.

4. Experimental results and discussion

Frequency spectral analyses of vibrations and audible noise emissions of the machine operating at full-load are carried out in the following discussion. First, the spectra of healthy machine are analysed as a reference point. Thereafter, spectra of the machine under particular faults are evaluated with the emphasis on the characteristic frequencies' amplitude rise or drop in comparison with the case of healthy machine. FFT is applied on the original recorded signals and no additional signal filtration is used. Considering the implemented faults vibration response, only low frequency (up to 200 Hz) spectra of radial vibrations are analysed in the

following discussion. To verify an assumption that audible noise emissions excited by the vibrations can be identified using smartphone, also the frequency spectra of audible noise are analysed in the same frequency range as the vibrations. The evaluated frequency range comprehends the rotational speed frequencies of order one to eight with the corresponding sidebands in the distance of pole passing frequency multiples and twice line frequencies of order one and two. Logarithmic scale of the vertical axis is used for amplitude representation in all figures.

Vibration signals have very similar frequency spectra in all measured positions, which allow making the analyses for all the faults in one position only. Spectra contain basically the same frequency components, which differ in amplitudes to some extent. Amplitude values of signals, measured by the particular vibration sensors, can be affected by the glue quantity used for the mounting of the sensors, or more precisely, by overall quality of the glued joints. By this reason, signals from the same sensor are evaluated in the paper. Similarly, audible noise signals from only one recording position are analysed.

Vertical mechanical support of the tested and loading machines has a number of natural frequencies in the analysed frequency bandwidth. Unfortunately, some sidebands of the 2nd, 3rd, 5th and 6th rotational speed harmonics are in a close vicinity of these natural frequencies, which is the main reason they have almost equal or even higher amplitude than particular rotational speed harmonics.

Some vibration frequencies in the spectra can also be excited by the loading machine fed by the frequency converter. However, the influence of loading machine should be the same in all the tests performed, and the experiment is based on the known frequency spectrum of the healthy machine and its comparison with the spectra of the machine with implemented faults.

4.1. Healthy machine

The vibration frequency spectrum of the healthy machine is presented together with the spectrum of the machine under dynamic eccentricity in Fig. 3. The most important frequencies for diagnostics visible in Fig. 3 are the rotational speed frequency f_{1x} , twice line frequency $2f_L$ and their harmonics. These frequency components with the exception of f_{6x} and f_{8x} are clearly visible even in the spectrum of the healthy machine.

Text in the boxes with green margins in Fig. 3 gives the information about frequency components marked with the corresponding green arrows. For example, the label $f_{4x} \pm 2sb @ f_p$ with five arrows means that the fourth harmonic of rotational frequency is marked with the central arrow. Two sidebands in the right side of f_{4x} (each shifted of $+f_p$) and in the left side (each shifted of $-f_p$) are marked with two arrows in the right and two arrows in the left respectively. In this particular case the first sideband in the right side of f_{4x} is in a close vicinity of twice line frequency and can be superimposed to it.

As seen in Figs. 4 and 5, the frequency spectra of audible noise signals recorded by Sony and Samsung smartphones are similar to the spectra of vibrations. In audible noise signal spectra, there is no such difference between amplitudes of characteristic frequencies and especially general noise at lower frequencies. In fact, f_{1x} , f_{2x} , f_{3x} , f_{6x} for both smartphones and f_{7x} for Sony are

indistinguishable from the general noise. Compared to the spectrum of vibrations, some sidebands are not visible in the spectra of audible noise signals either.

4.2. Dynamic eccentricity (DEC)

A very important vibration amplitude can be found at the rotational speed frequency f_{1x} , which is almost ten times higher for the machine under dynamic eccentricity than in the case of the healthy machine. There is also a noticeable rise in the amplitude of f_{5x} , f_{6x} and f_{7x} rotational speed frequency harmonics. On the other hand, there is an amplitude drop in f_{4x} , f_{2L} and f_{4L} . Vibrations at other frequencies have similar amplitudes as in the healthy machine. Dynamic eccentricity/healthy machine amplitude ratios of vibration and audible noise signals for all characteristic frequencies are listed in Table 2. There is also a significant rise in amplitudes of certain sidebands, however some of these sidebands are in a close vicinity of natural frequencies of mechanical support as stated above.

Table 2 Amplitude ratios of DEC/healthy machine

	f_{1x}	f_{2x}	f_{3x}	f_{4x}	f_{2L}	f_{5x}	f_{6x}	f_{7x}	f_{8x}	f_{4L}
Vibrations	9.99	1.05	1.29	0.51	0.56	2.24	7.35	3.59	1.09	0.53
Sony	4.82	2.51	0.62	0.82	1.69	1.26	0.88	2.73	0.75	1.65
Samsung	4.51	0.93	0.92	0.39	0.44	0.49	0.39	0.29	0.35	0.27

Comparing the vibrations and audible noise signals frequency spectra, one can notice similarity in frequency components between the spectra, as in case of the healthy machine. Also, audible noise signals have a significantly higher amplitude at rotational speed fundamental frequency. The dynamic eccentricity/healthy amplitude ratio of audible noise signals is 4.82 for Sony and 4.51 for Samsung smartphones. Amplitude rise of f_{2x} , f_{5x} and f_{7x} components is found only in the signal measured by Sony for dynamic eccentricity.

In opposite to the vibration frequency spectra, there is an amplitude rise in twice line frequency component f_{2L} and its harmonic f_{4L} in the audible noise signal frequency spectrum recorded by Sony. However, the signal recorded by Samsung has an amplitude drop at these frequencies again.

4.3. Broken rotor bars

Comparison of the machine with different number and position of broken rotor bars and the healthy machine is performed in this section. Individual cases are marked as follows:

- 1BB – one broken bar;
- 2BB – two consecutive broken bars;
- 3BB – three consecutive broken bars;
- 1x2BB – two broken bars (four healthy bars in between).

Since both, vibration and audible noise signals frequency spectra, are similar to those presented in Figs. 3 to 5, only changes in amplitude values are pointed out in the following discussion. Faulty/healthy amplitude ratios of the cases mentioned above are presented in Tables 3 to 6.

Vibrations in all the machines with broken rotor bars increase at all rotational speed harmonics with the exceptions of f_{4x} , which significantly drops or remains the same in case of 3BB. Very significant rise is noted in f_{5x} , f_{6x} and f_{7x} . A special case is 2BB, where vibrations at f_{1x} are almost equal

to the healthy machine, however, vibrations at other rotational speed harmonics are substantially higher. Vibrations at twice line frequency rise with the number of consecutive broken rotor bars, but for 1x2BB they slightly decrease.

Comparing audible noise signals, the ones recorded by Samsung phone have generally higher faulty/healthy amplitude ratio at f_{1x} , f_{2x} and f_{3x} frequency components, whilst the ones recorded by Sony phone have a higher amplitude ratio at higher frequencies.

Assuming f_{1x} as the most typical frequency for broken rotor bar diagnostics, suitability of Sony smartphone as diagnostic tool cannot be concluded in the case of 3BB only by presented measurements. On the other hand, Samsung smartphone records signals with sufficiently higher f_{1x} amplitude in all broken bar cases.

Table 3 Amplitude ratios of 1BB/healthy machine

	f_{1x}	f_{2x}	f_{3x}	f_{4x}	f_{2L}	f_{5x}	f_{6x}	f_{7x}	f_{8x}	f_{4L}
Vibrations	3.51	2.28	0.98	0.06	1.28	11.67	5.71	7.13	14.59	0.93
Sony	1.57	1.28	0.27	1.04	1.67	0.94	0.65	1.41	0.94	3.30
Samsung	2.16	0.82	0.62	0.86	0.78	0.67	0.33	0.56	0.67	1.39

Table 4 Amplitude ratios of 2BB/healthy machine

	f_{1x}	f_{2x}	f_{3x}	f_{4x}	f_{2L}	f_{5x}	f_{6x}	f_{7x}	f_{8x}	f_{4L}
Vibrations	1.07	2.60	3.37	0.39	2.16	12.06	47.21	6.46	2.08	0.78
Sony	1.19	1.05	0.33	0.92	1.40	1.49	1.53	1.92	0.81	1.02
Samsung	1.51	1.37	0.45	0.89	0.59	0.86	0.36	0.27	0.73	0.59

Table 5 Amplitude ratios of 3BB/healthy machine

	f_{1x}	f_{2x}	f_{3x}	f_{4x}	f_{2L}	f_{5x}	f_{6x}	f_{7x}	f_{8x}	f_{4L}
Vibrations	5.66	13.28	4.24	0.96	2.63	86.15	35.06	21.94	10.16	0.90
Sony	0.96	1.10	0.42	0.69	2.12	5.60	0.99	81.17	0.18	1.80
Samsung	3.69	2.16	0.59	0.83	1.26	6.00	0.38	16.27	0.82	0.76

Table 6 Amplitude ratios of 1x2BB/healthy machine

	f_{1x}	f_{2x}	f_{3x}	f_{4x}	f_{2L}	f_{5x}	f_{6x}	f_{7x}	f_{8x}	f_{4L}
Vibrations	8.55	3.66	1.39	0.06	0.90	7.77	55.72	10.47	2.55	0.79
Sony	4.14	0.52	1.21	0.87	1.66	1.02	2.57	4.79	1.64	3.09
Samsung	8.10	0.51	1.25	0.49	0.53	0.77	0.77	0.73	0.55	1.68

4.4. Fault combinations

Analyses of the machines with a combination of implemented faults are carried out below. Studied fault combinations are:

- DEC_1x2BB – dynamic eccentricity and two broken bars (four healthy bars in between);
- DEC_1x2BB_LB – dynamic eccentricity, two broken bars (four healthy bars in between) and loose bearing.

Considering the similarity of frequency spectra, only amplitude ratios of faulty/healthy machines are evaluated again. Amplitude ratio values are summarized in Tables 7 and 8.

In case of DEC_1x2BB, vibrations increase at all rotational speed harmonics but f_{4x} again. Amplitude of f_{1x} is significantly higher than in case of the healthy machine, but at the same time, substantially lower than in the cases of individual DEC and 1xBB faults. This can be caused by

different direction of unbalanced magnetic pull components excited by DEC and 1x2BB.

Vibrations of machine under DEC_1x2BB_LB fault combination have higher amplitude at all rotational speed frequency harmonics, including f_{4x} . This is, therefore, the only faulty case in presented measurements, in which vibration amplitude rise at f_{4x} is noted. Vibrations rise at this particular frequency is caused obviously by the loose bearing. There is also significant rise in amplitudes at f_{2x} and f_{3x} , which is comparable to 3BB case only.

Based on audible noise signals, one cannot differentiate between DEC_1x2BB and DEC_1x2BB_LB faulty cases since both have considerable amplitude rise at f_{2x} and f_{3x} . Only f_{3x} recorded by Sony in DEC_1x2BB has an amplitude drop.

Table 7 Amplitude ratios of DEC_1x2BB/healthy machine

	f_{1x}	f_{2x}	f_{3x}	f_{4x}	f_{2L}	f_{5x}	f_{6x}	f_{7x}	f_{8x}	f_{4L}
Vibrations	4.85	2.05	1.73	0.62	1.38	6.51	3.74	14.05	4.86	0.90
Sony	2.19	1.97	0.55	0.75	1.18	1.47	0.88	4.02	1.23	0.88
Samsung	5.86	1.88	2.06	1.14	0.44	1.98	0.59	0.67	0.96	0.75

Table 8 Amplitude ratios of DEC_1x2BB_LB/healthy machine

	f_{1x}	f_{2x}	f_{3x}	f_{4x}	f_{2L}	f_{5x}	f_{6x}	f_{7x}	f_{8x}	f_{4L}
Vibrations	7.75	15.41	5.60	5.97	1.60	9.98	49.17	15.56	9.90	0.59
Sony	3.19	2.93	2.65	0.91	1.86	2.57	6.39	11.05	1.03	1.83
Samsung	7.74	1.69	2.11	0.49	0.66	1.07	1.15	1.25	0.37	0.66

Graphical representation of values in Tables 2 to 8 are shown in Fig. 6 for vibration signals, in Fig. 7 for audible noise signals recorded by Sony Xperia Go and in Fig. 8 for audible noise signals recorded by Samsung Galaxy S4 mini.

4.5. Neural network validation

To assess the feasibility of smartphone recorder possibilities for the usage in electrical machine fault detection, as well as possibilities for further automation through pattern recognition and signal processing, a simple two layer neural network was composed. MATLAB software was used for this purpose.

Fig. 9 presents the confusion matrix of fault detection through smartphone recorded sound files. Overall fault detection probability according to the composed neural network is 96.4%. Faults in output and target classes are numbered the same way as in chapter 2 of the paper.

Correctly classified fault files are located on the main diagonal of the confusion matrix (green cells). Wrongly classified files are outside of the main diagonal (red cells). The percentages in green show the overall correct classified faults. Red ones show the wrong classification percentage related to each fault. The upper number in the cells shows the number of files classified to this fault.

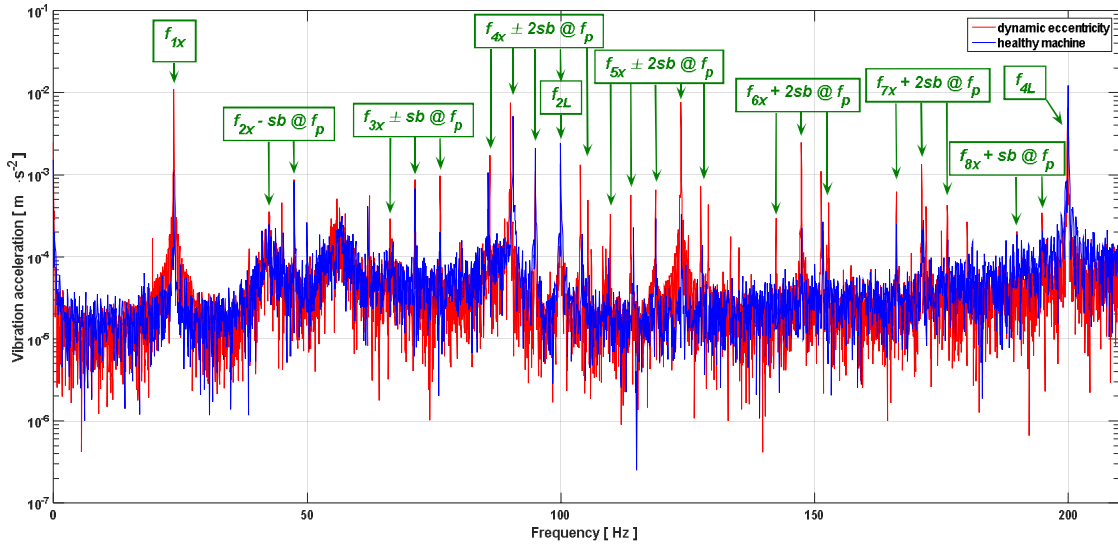


Fig. 3. Vibration frequency spectra of healthy machine and machine under dynamic eccentricity

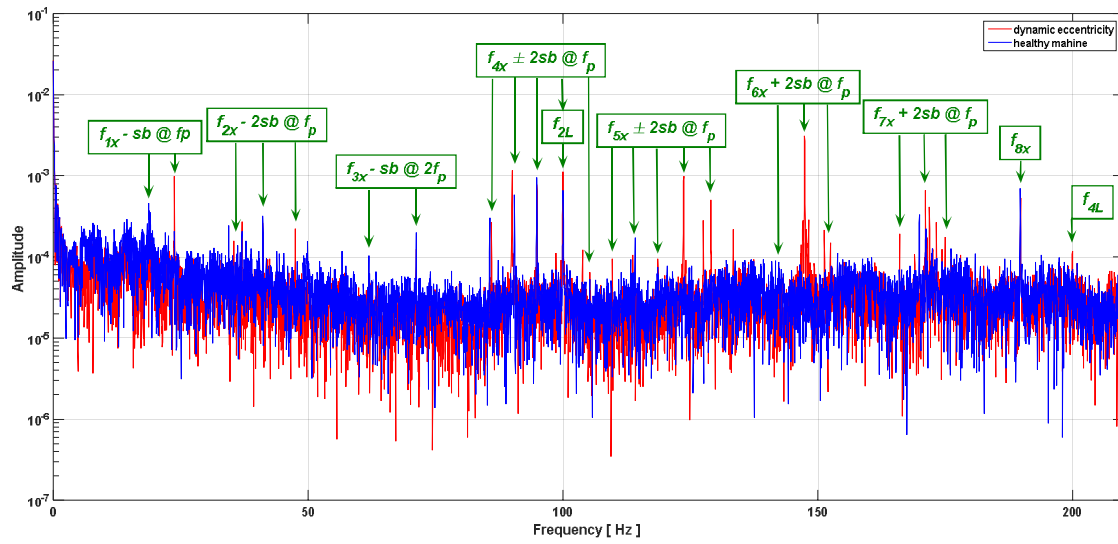


Fig. 4. Frequency spectra of audible noise signals of healthy machine and machine under dynamic eccentricity recorded by Sony Xperia Go

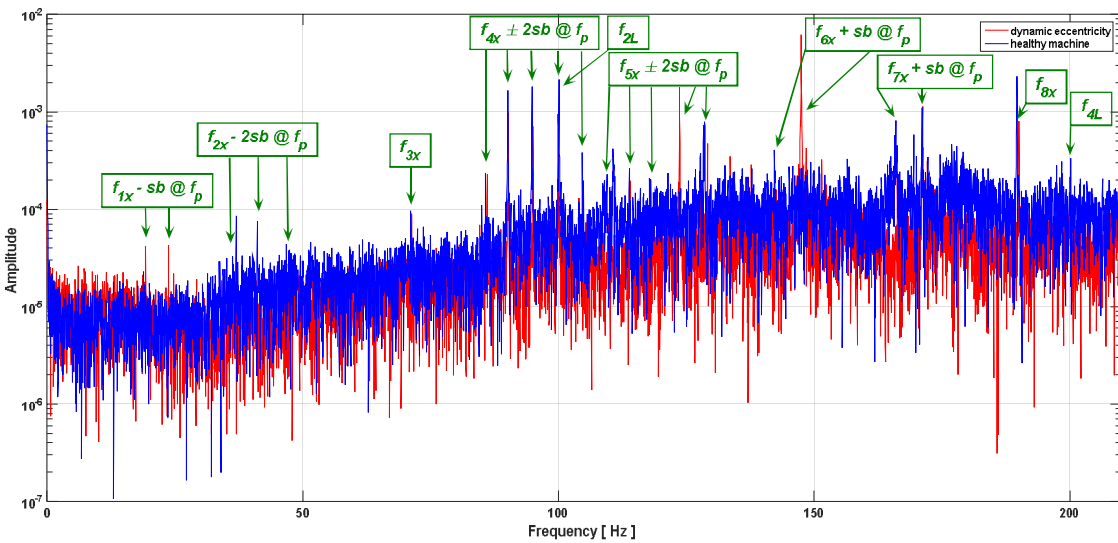


Fig. 5. Frequency spectra of audible noise signals of healthy machine and machine under dynamic eccentricity recorded by Samsung Galaxy S4 mini

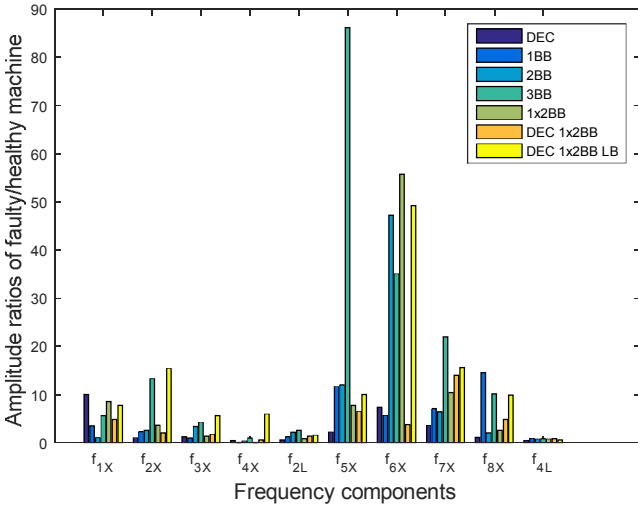


Fig. 6. Vibration signals amplitude ratios of faulty/healthy machines

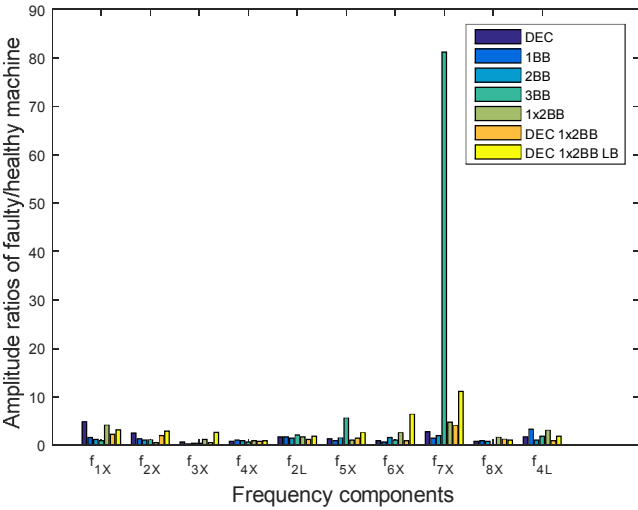


Fig. 7. Audible noise signals amplitude ratios of faulty/healthy machines recorded by Sony smartphone

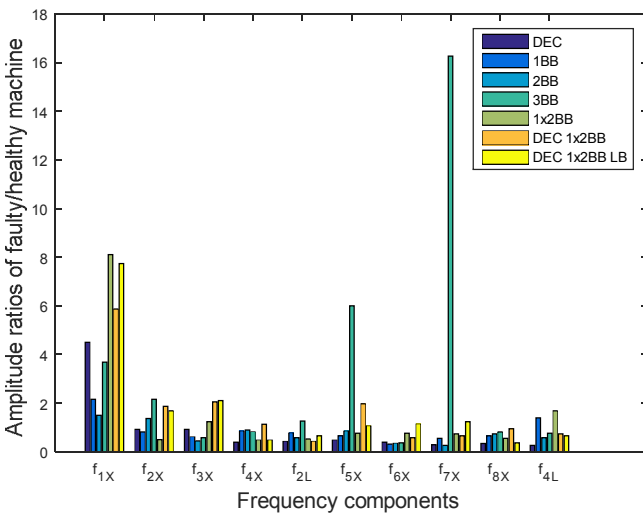


Fig. 8. Audible noise signals amplitude ratios of faulty/healthy machines recorded by Samsung smartphone

Output Class	1	2	3	4	5	6	7	8	
1	111 11.8%	2 0.2%	1 0.1%	0 0.0%	0 0.0%	5 0.5%	0 0.0%	0 0.0%	93.3% 6.7%
2	0 0.0%	95 10.1%	0 0.0%	0 0.0%	0 0.0%	0 0.0%	0 0.0%	2 0.2%	97.9% 2.1%
3	1 0.1%	0 0.0%	106 11.3%	0 0.0%	0 0.0%	0 0.0%	0 0.0%	0 0.0%	99.1% 0.9%
4	0 0.0%	1 0.1%	4 0.4%	124 13.2%	0 0.0%	0 0.0%	0 0.0%	0 0.0%	96.1% 3.9%
5	0 0.0%	1 0.1%	0 0.0%	1 0.1%	122 13.0%	2 0.2%	2 0.2%	1 0.1%	94.6% 5.4%
6	0 0.0%	0 0.0%	0 0.0%	0 0.0%	0 0.0%	119 12.7%	1 0.1%	0 0.0%	99.2% 0.8%
7	0 0.0%	1 0.1%	1 0.1%	0 0.0%	0 0.0%	1 0.1%	108 11.5%	2 0.2%	95.6% 4.4%
8	2 0.2%	0 0.0%	1 0.1%	0 0.0%	0 0.0%	1 0.1%	1 0.1%	118 12.6%	95.9% 4.1%
	97.4% 2.6%	95.0% 5.0%	93.8% 6.2%	99.2% 0.8%	100% 0.0%	93.0% 7.0%	96.4% 3.6%	95.9% 4.1%	96.4% 3.6%
	1	2	3	4	5	6	7	8	

Fig. 9. Confusion matrix of fault detection through smartphone recorded sound files. Overall fault detection probability is 96.4%.

5. Conclusion

Since all implemented faults excite vibrations basically at the same frequencies, the amplitude rise or drop of particular frequency components in comparison with the healthy machine is accentuated in provided analyses. Significant vibration amplitude rise at rotational speed frequency and all its harmonics but f_{4x} is noticed in all faulty states, due to unbalanced magnetic pull caused by dynamic eccentricity or/and broken rotor bars.

A rather surprising result is found at the analysis of 2BB faulty state, where very small rotational speed fundamental f_{1x} amplitude rise is recorded. Similarly, small amplitude rise is recorded in all measuring positions, which exclude the vibration sensor error. However, the other rotational speed harmonics rise substantially in amplitude and can be used for machine diagnostics.

Focusing on rotational speed fundamental f_{1x} as the main vibration frequency spectrum component for revolving unbalanced magnetic pull diagnostics, higher vibrations amplitude, caused by dynamic eccentricity, than the ones caused by broken rotor bar cases, can be seen in the analyses results. Including only broken rotor bars, the highest vibrations amplitude rise is in 1x2BB case, followed by 3BB and 1BB. Different f_{1x} vibrations amplitude rise in the machine under DEC_1x2BB and DEC_1x2BB_LB fault combinations is caused mainly by different positions of radial magnetic forces, caused by dynamic eccentricity and broken rotor bars.

The assumption, that loose bearing excites vibrations at f_{2x} and f_{3x} rotational speed harmonics, is confirmed in the analyses as well. Vibrations amplitude rise at these frequencies is the highest in DEC_1xBB_LB case, closely followed by 3BB. However DEC_1xBB_LB is the only case, where f_{4x} harmonic does not drop, but significantly rises instead.

In frequency spectra of audible noise signals recorded by both Sony and Samsung smartphones, only f_{1x} component

rises significantly in all faulty cases. The only exception is f_{1x} component recorded by Sony in case of 3BB fault, which is slightly lower than for the healthy machine. However, the same frequency component, recorded by Samsung, rises substantially in this particular case. In the case of DEC_1x2BB_LB fault combination, f_{2x} and f_{3x} amplitude rise is noticed in signals recorded by both smartphones.

Compared to vibrations, audible noise signals have generally lower faulty/healthy amplitude ratio. This can be caused by the fact that audible noise signals are measured in a certain distance from the machine, whilst vibration sensors are firmly fastened to the machine frame. Recorded audible noise signals can also be affected by sound reflection or refraction.

Comparing faulty/healthy amplitude ratios of signals recorded by Sony and Samsung, the ones recorded by Samsung have generally higher ratios at lower frequencies, whilst the ones recorded by Sony have higher ratios at higher frequencies. This can be justified by different frequency response of the microphones used in particular smartphones.

All in all, it can be concluded, that smartphones, or rather any recording portable device, can be used for simple preliminary condition monitoring, as the rises in fault indicating harmonics can be detected. This is also backed by the neural network analysis, in which the fault detection probability of 96.4% was achieved.

Further investigation is needed for the analysis options of various phones or recording devices. Emphasis must be put to the microphones used in the tests, as the filtration level and frequency response of mobile phone microphones is varying by brand and type of the device, and information on these components is not generally available for public. Also, automation of electrical machine diagnostics using smartphones should be considered. Applications, using signal processing and pattern recognition algorithms for preliminary testing are to be constructed and analysed.

6. Acknowledgments

This work was supported by the Estonian Research Council under grant PUTJD134, European Regional Development Fund under Mobilias Plus programme returning researcher grant MOBTP13 and by the funding program of the University of West Bohemia number SGS-2015-038.

7. References

- [1] Cabal-Yepez, E., Garcia-Ramirez, A. G., Romero-Troncoso, R. J., Garcia-Perez, A., Osornio-Rios, R. A.: 'Reconfigurable monitoring system for time-frequency analysis on industrial equipment through STFT and DWT', *IEEE Transactions on Industrial Informatics*, 2013, 9, (2), pp. 760-771
- [2] Nandi, S., Ilamparithi, T. C., Lee, S. B., Hyun, D.: 'Detection of eccentricity faults in induction machines based on nameplate parameters', *IEEE Transactions on Industrial Electronics*, 2011, 58, (5), pp. 1673-1683
- [3] Yan, R., Gao, R. X., Chen, X.: 'Wavelets for fault diagnosis of rotary machines: A review with applications', *Signal Processing*, 2014, 96, pp. 1-15
- [4] Seshadrinath, J., Singh, B., Panigrahi, B. K.: 'Investigation of vibration signatures for multiple fault diagnosis in variable frequency drives using complex wavelets', *IEEE Transactions on Power Electronics*, 2014, 29, (2), pp. 936-945
- [5] Kankar, P. K., Sharma, S. C., Harsha, S. P.: 'Fault diagnosis of rolling element bearing using cyclic autocorrelation and wavelet transform', *Neurocomputing*, 2013, 110, pp. 9-17
- [6] Konar, P., Chattopadhyay, P.: 'Bearing fault detection of induction motor using wavelet and support vector machines (svms)', *Applied Soft Computing*, 2011, 11, (6), pp. 4203-4211
- [7] Rafiee, J., Fafiee, M. A., Tse, P. W.: 'Application of mother wavelet functions for automatic gear and bearing fault diagnosis', *Expert Systems with Applications*, 2010, 37, (6), pp. 4568-4579
- [8] Lei, Y., Lin, J., He, Z., Zuo, M. J.: 'A review on empirical mode decomposition in fault diagnosis of rotating machinery', *Mechanical Systems and Signal Processing*, 2013, 35, (1-2), pp. 108-126
- [9] Zheng, J., Cheng, J., Yang, Y.: 'Generalized empirical mode decomposition and its applications to rolling element bearing fault diagnosis', *Mechanical Systems and Signal Processing*, 2013, 40, (1), pp. 136-153
- [10] Zhang, X., Zhou, J.: 'Multi-fault diagnosis for rolling element bearings based on ensemble empirical mode decomposition and optimized support vector machines', *Mechanical Systems and Signal Processing*, 2013, 41, (1-2), pp. 127-140
- [11] Bin, G. F., Gao, J. J., Li, X. J., Dhillon, B. S.: 'Early fault diagnosis of rotating machinery based on wavelet packets – Empirical mode decomposition feature extraction and neural network', *Mechanical Systems and Signal Processing*, 2012, 27, pp. 696-711
- [12] Amarnath M., Krishna, I. R. P.: 'Empirical mode decomposition of acoustic signals for diagnosis of faults in gears and rolling element bearings', *IET Science, Measurement and Technology*, 2012, 6, (4), pp. 279-287
- [13] Yan J., Lu, L.: 'Improved Hilbert-Huang transform based weak signal detection methodology and its application on incipient fault diagnosis and ECG signal analysis', *Signal Processing*, 2014, 98, pp. 74-87
- [14] Cheng, G., Cheng, Y. L., Shen, L. H., Qiu, J. B., Zhang, S.: 'Gear fault identification based on Hilbert-Huang transform and SOM neural network', *Measurement*, 2013, 46, (3), pp. 1137-1146
- [15] Osman, S., Wang, W.: 'An enhanced Hilbert-Huang transform technique for bearing condition monitoring', *IET Measurement, Science and Technology*, 2013, 24, (8), pp. 1-13

- [16] Kang, M., Kim, J., Kim, J. M.: 'High-performance and energy-efficient fault diagnosis using effective envelope analysis and denoising on a general-purpose graphics processing unit', *IEEE Transactions on Power Electronics*, 2015, 30, (5), pp. 2763-2776
- [17] Belahcen, A., Gyftakis, K., Martinez, J., Climente-Alarcon, V., Vaimann, T.: 'Condition monitoring of electrical machines and its relation to industrial internet', *Proc. IEEE Workshop on Electrical Machines Design, Control and Diagnosis (WEMDCD)*, Torino, Italy, March 2015, pp. 233-241
- [18] Belahcen, A., Martinez, J., Vaimann, T.: 'Comprehensive computations of the response of faulty cage induction machines', *Proc. International Conference on Electrical Machines (ICEM)*, Berlin, Germany, September 2014, pp.1510-1515
- [19] Vaimann, T., Belahcen, A., Kallaste, A.: 'Necessity for implementation of inverse problem theory in electric machine fault diagnosis', *Proc IEEE 10th International Symposium on Diagnostics for Electrical Machines, Power Electronics and Drives (SDEMPED)*, Guarda, Portugal, September 2015, pp. 380-385
- [20] Rzeszucinski, P., Orman, M., Pinto, C., Tkaczyk, A., Sulowicz, M.: 'A signal processing approach to bearing fault detection with the use of a mobile phone', *Proc. IEEE 10th International Symposium on Diagnostics for Electrical Machines, Power Electronics and Drives (SDEMPED)*, Guarda, Portugal, September 2015, pp. 310-315
- [21] Finley, J. W. R., Hodowanec, M. M., Holter, W. G.: 'An analytical approach to solving motor vibration problems', *IEEE Transactions on Industry Applications*, 2000, 36, (5), pp.1467-1480
- [22] Sobra, J., Vaimann, T., Belahcen, A.: 'Mechanical vibration analysis of induction machine under dynamic rotor eccentricity', *Proc. 17th International Scientific Conference on Electric Power Engineering*, Prague, Czech Republic, May 2016, pp.413-416
- [23] Sobra, J., Kindl V., Skala, B. 'Determination of the force caused by broken rotor bar and static eccentricity in an induction machine', *Proc. ELEKTRO 2014*, Rajecké Teplice, Slovakia, May 2014, pp. 375-378
- [24] Application notes, 'Vibration diagnostics for industrial electric motor drives', Brüel & Kjaer Sound & Vibration Measurement A/S, Naerum, Denmark, 1988.